# Evaluating the stray current corrosion of steel rebar in different layouts

Chen, Zhipei; Gao, Liang; Koleva, Dessi A.

**Important note**
To cite this publication, please use the final published version (if applicable).
Please check the document version above.

# Evaluating the stray current corrosion of steel rebar in different layouts

Zhipei Chen [a,*], Liang Gao [a], Dessi A. Koleva [b]

[a] *School of Civil Engineering, Beijing Jiaotong University, 100044 Beijing, China*
[b] *Microlab, Department 3MD, Faculty of Civil Engineering and Geosciences, Delft University of Technology, Stevinweg 1, 2628 CN Delft, the Netherlands*

ARTICLE INFO

ABSTRACT

By different testing methods (electrochemical techniques, potential shift monitoring, and Environmental Scanning Electron Microscope), this research evaluates the stray current corrosion of steel rebar in different layouts. The more significant corrosion state is observed when the steel bar is parallel to stray current flow, compared to the situation as a steel bar is vertical to the stray current. These outcomes are further clarified by the recorded level of stray current picked-up by steel rebar. It is found that the level of current actually picked-up by the steel rebar is decreasing. At the instant when the stray current supply is just turned off, an opposite current flow (back flow) is recorded. Besides an expansion of the database for monitoring stray current interference on reinforced concrete structures, the recorded results can be the basis for better understanding the process of stray current interference.

## 1. Introduction

Currents flowing along paths not being elements of purpose-built electric circuit, are called stray currents [1,2]. When the technical revolution with emergence of electric traction was launched (at the end of the 19th and beginning of the 20th century), the world was confronted with accelerated corrosion due to stray currents [3]. Later, with the intensive development of the petroleum and gas industry, corrosion of buried oil/gas pipelines induced by stray current has been found more and more frequently. Besides electrified traction systems, stray current may also originate from offshore structures, marine platforms, cathodic protection systems, etc [4–7]. Stray currents can also flow into and circulate in reinforced concrete structures near the above power sources [8,9].

As a kind of typical composite, steel rebar reinforced concrete is the most widely used building materials all over the world. The bond between the rebar surface and the surrounding concrete "combines" the rebar and concrete, making the bond strength of the steel-concrete interface an important property for reinforced concrete structures. Stray current circulating within the reinforced concrete can deteriorate the bond of steel-concrete interface [10]. In these cases, the concrete pore solution acts as an electrolyte, and the reinforcing steel embedded in concrete act as conductors, which can "pick up" the stray current and can corrode. At the location the stray current flows out from the reinforcement into the surrounding concrete matrix, anodic polarization/

reaction (steel corrosion) takes place. Stray current corrosion is one of the most severe damage forms for buried structures (such as tunnels and underground pipelines), as the matrix surrounding the metal (soil or concrete cover surrounding steel rebar) can offer a conductive path for the stray current [11]. However, the specific process of stray current corrosion on reinforced concrete is still unclear and less reported. Identical and reliable testing methods for evaluating or monitoring stray current corrosion are missing. This research aims to be a step forward for better understanding the stray current corrosion of reinforcing steel embedded in cement-based materials.

As is well-known in construction engineering, the layout of reinforcing steel embedded in concrete elements is usually steel rebar cage. An example (a metro segment) for this scenario is shown in Fig. 1 [12]. In this case, the stray current flowing in the tunnel segments can be parallel or vertical to the steel rebar. To study the stray current-induced corrosion for steel in concrete, although various works reported different aspects [13–19], the effects of the steel rebar layout on the amount and distribution of stray current corrosion product are still not investigated sufficiently. This aspect is of significance in view of the degree of corrosion damage, and geometrical location of corrosion product accumulation on the steel rebar surface. To clarify this aspect, two geometrical positions of the reinforcement embedded in mortar are tested - the steel bar placed parallel or vertical to the flow of the stray current. The stray current conditions are simulated in both Cl-free (in water) and Cl-containing (in 5% NaCl solution) mediums.

---

\* Corresponding author.
*E-mail address:* zhipeichen@outlook.com (Z. Chen).

A more corrosive state is observed when the steel bar is parallel to the current direction, compared to the situation of a rebar perpendicular to the stray current. This phenomenon is further clarified via additional series of tests, where the picked-up stray current level and potential shift of the rebar undergoing stray current are monitored. Another aim of this series of tests is to better understand the time-dependent process of stray current interference on the steel, in the period of stray current supply as well as after stray current cut-off. This time-dependent response of a steel rebar undergoing stray current is rarely studied before. It is found that, though the supplying stray current is constant, the level of current picked-up by the steel rebar is decreasing. At the instant when the stray current supply is just turned off, an opposite current flow (back flow) is monitored. This is caused by the stray current-induced potential difference between anode and cathode.

## 2. Experimental

### 2.1. Materials and specimens

The experimentally investigated specimens in this work are also reinforced mortar cubes ($40 \times 40 \times 40$ mm$^3$). The specimens were cast from Ordinary Portland cement CEM I 42.5 N and normed sand. The Binder/Sand ratio and Water/Binder ratio were 1:3 and 0.5, respectively. The embedded steel was type FeB500HKN (d = 6 mm), with exposed length of 20 mm. The rebar pieces were centrally and fully embedded in the mortar cubes in two layouts - rebar placed parallel or vertical to the stray current direction (see Fig. 2).

After casting, the specimens were cured in a fog room (98% RH, 20 °C) for 24 h (24 h). After demoulding at age of 24 h, the specimens were lab-conditioned (treated in lab air). The relevant conditions and specimen designations are summarized in Table 1. Each group (with the same steel layout and conditioning) had 2 replicate specimens.

Supply of stray current (level of 3 mA/cm$^2$) started at 24 h of age in the relevant conditions (the current density was calculated according to the exposed steel surface area). It has been reported that stray alternating current (AC) induced corrosion is moderate compared to stray direct current (DC) induced corrosion. According to related research, a critical AC current density of 30 A/m$^2$ (=3mA/cm$^2$) was suggested, above which the corrosion would be significant [1,2]. Hence in this work, the stray DC density of 3 mA/cm$^2$ was supplied, to ensure that the stray current can induce remarkable corrosion on steel surface. The configurations for supplying stray current are shown in Fig. 2: two cast-in MMO Ti meshes ($40 \times 40$ mm$^2$) are used as poles for stray current supply. The conditioning of these specimens, specifically with respect to the stray current application, was performed in two phases: Phase 1 - 24 h (1 day) to 28 days; Phase 2 - 72 days to 123 days. Over 28–72 days, the continuous stray current supply was cut off, the specimens were placed in water or 5% NaCl solution only. The reason for the interruption of

continuous stray current is to ensure the stability of the electrochemical state of steel surface over 28 days to 72 days. Over this period, the short-term (only about 1500 s) stray current application would be supplied, to monitor the potential shifts of steel rebar due to short-term stray current. If the continuous stray current interference was still on steel, the potential of steel would be unstable due to continuous stray current. In this unstable state of steel rebar, the monitoring of potential shifts of steel rebar undergoing short-term stray current would be not feasible. At 34 days of age, the above-mentioned additional tests were performed (the details of these tests can be seen in Section 2.2.2), with the aim to monitor the potential shifts of steel rebar due to short-term stray current application.

### 2.2. Testing methods

#### 2.2.1. Electrochemical tests

Electrochemical tests, including Linear Polarization Resistance (LPR), Electrochemical Impedance Spectroscopy (EIS) and Potentio-Dynamic Polarization (PDP) were conducted at Open Circuit Potential (OCP) for all specimens. LPR, EIS and PDP were conducted in general 3-electrode system: counter electrode was the two Ti electrodes (connected with each other), working electrode was steel rebar, and reference electrode was an external Saturated Calomel Electrode (SCE). Prior to and during the electrochemical tests the specimens were immersed fully in the relevant aqueous medium (in water or 5% NaCl) for 24 h, i.e., a 24-hour potential decay. The aim of this is to result in stability of the electrochemical state of steel (i.e., achieve a stable OCP), so that electrochemical tests can follow after the decay. Within electrochemical tests, the specimens were also immersed fully in the relevant medium (in water or 5% NaCl). To make sure the execution of electrochemical tests on fully embedded steel rebar, a connection between steel rebar and wire (wire with a terminal, the terminal is above the liquid level) is necessary. To this end, a screw hole was drilled at end of rebar for connecting with a bolt, to obtain a stable connection between steel rebar and wire. To seal this connection, epoxy resin covered the whole junction. The real picture of this wire/terminal can be seen in Fig. 4c.

LPR was performed at intervals of 14, 102 and 123 days, in the range of ±20 mV (vs OCP), at a scan rate of 0.1 mV/s. EIS and PDP were performed at the end of conditioning (123 days). In order to account for a more accurate assessment of the bulk matrix characteristics, the EIS tests here were conducted in the maximum frequency range (i.e., 1 MHz-10 mHz) can be supported by the instrument, by superimposing an AC voltage of 10 mV (rms). In this work EIS was performed in the full (instrument-determining) frequency range (as abovementioned - of 1 MHz to 10 mHz), to offer information for both the property of the bulk matrix (high to middle frequency - HF to MF range of EIS) and the electrochemical response of the embedded steel (low frequency - LF range of EIS). In order to collect additional information of the electrochemical
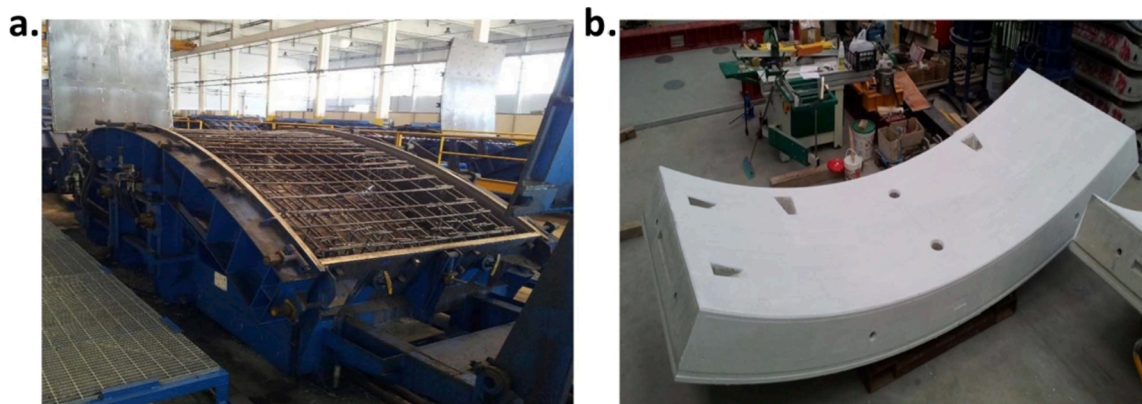


**Fig. 1.** Metro segment: (a). reinforcing steel cage before casting; (b). after casting [12].
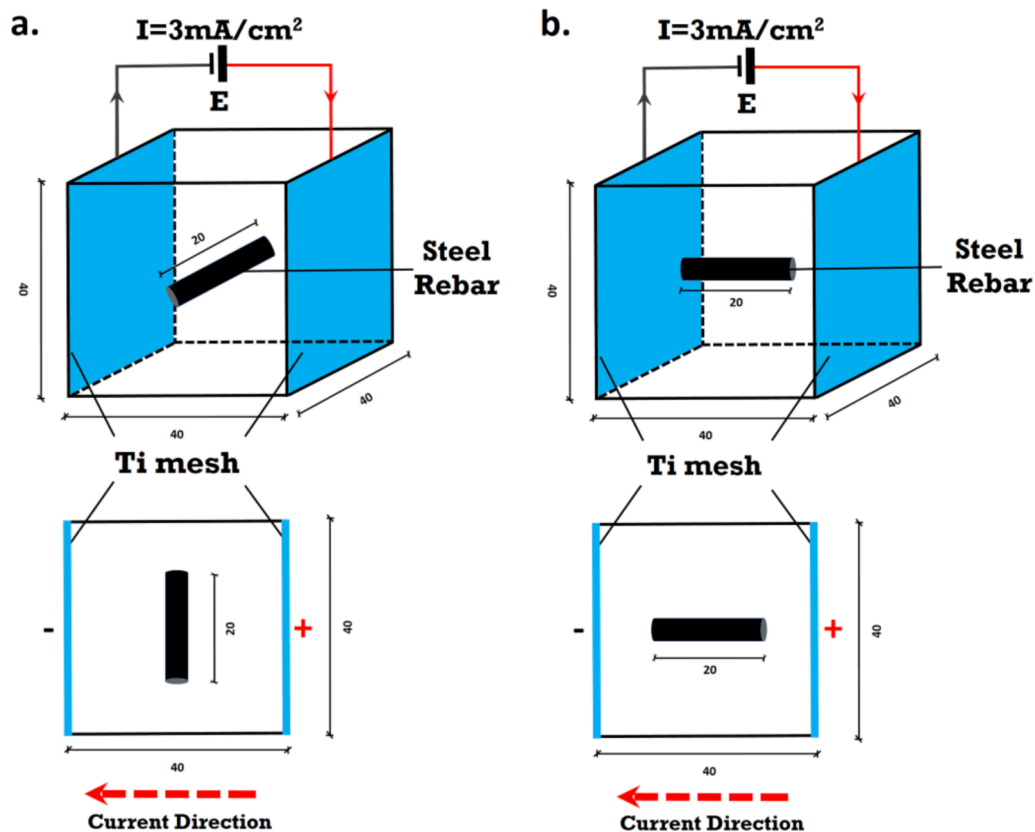
**Fig. 2.** Schematic and top-view of test specimen and setup for stray current supply and position of electrodes: (a) Steel bar vertical to stray current; (b) Steel bar parallel to stray current.

**Table 1**
Specimens' designations and relevant conditions summary.

| Groups | Specimen Designation | Immersion (1/2nd of height) | Rebar Layout (to stray current direction) |
|--------|---------------------|----------------------------|-------------------------------------------|
| S(V) | S(V)-1 | Water | Vertical |
| | S(V)-2 | Water | Vertical |
| S(P) | S(P)-1 | Water | Parallel |
| | S(P)-2 | Water | Parallel |
| CS(V) | CS(V)-1 | 5% NaCl | Vertical |
| | CS(V)-2 | 5% NaCl | Vertical |
| CS(P) | CS(P)-1 | 5% NaCl | Parallel |
| | CS(P)-2 | 5% NaCl | Parallel |

state of the steel surface, PDP was finally performed in the range of $-0.15$ V to $+0.90$ V (vs OCP) at a scan rate of 0.5 mV/s. The used equipment for electrochemical tests in this work was Metrohm Autolab (Potentiostat PGSTAT302N), combined with a FRA2 module.

*2.2.2. Potential change monitoring on individual specimens*

At the age of 34 days (between Phase 1 and Phase 2, when the continuous stray current supply was off), stray current was supplied on selected samples for about 1500 s, to monitor the potential change of the embedded steel undergoing stray current. This monitoring test was conducted on S(V)-1 and S(V)-2 specimens. The schematic and top-view of the specimens and the reference electrode arrangement for potential shift monitoring on individual specimens are depicted in Fig. 3.

Stray current induces both cathodic and anodic polarization on the steel surface, because of the inflow and outflow respectively. So the shift of the overall (mixed) potential induced by stray current flow reflects the
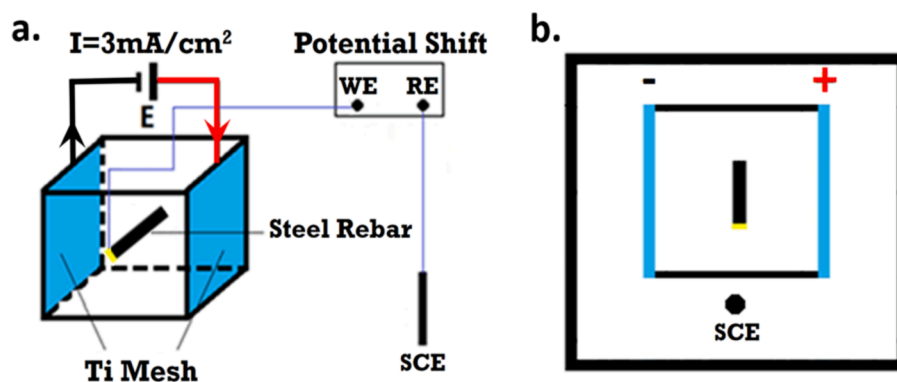


**Fig. 3.** (a) Schematic, and (b) top-view, of specimen and reference electrode arrangement for potential shift monitoring on individual specimens.

intensity of stray current interference. The aim of this test was to monitor the potential shifts (ON and OFF potentials) of the rebar undergoing stray current, and the potential decay after stray current supply. The IR drop involved in the potential shift of rebar was also recorded and will be discussed.

*2.2.3. Picked-up current levels in a stray current electrical field*

In practice, only part of the stray current can flow into a reinforced concrete element. To simulate the situation where part of the stray current flows in the external medium, while the other part flows into the reinforced structure, the specific set-up was adopted and presented in Fig. 4. Two external electrodes (Ti meshes) were used as terminals for current supply, and to produce a stray current electrical field. Two reinforced mortar cubes were placed in this stray current electrical field. These tests were performed at the end of test period (after 123 days of conditioning). This series of the testing procedures were conducted on specimens CS(P)-1 and CS(P)-2 in 5% NaCl solution (fully immersed).

As shown in Fig. 4, two pieces of steel rebars were coupled to each other, as anode and cathode according to the direction of stray current supply. The aim of this arrangement is to identify the behavior of anodic/cathodic polarization during stray current supply. The electrode potential change of the rebar undergoing stray current electrical field was recorded. The current level picked-up by steel (the stray current flowing into the two pieces of steel rebars) was also obtained, by



**Fig. 4.** Basic testing arrangement for simulation of practical stray current electric field: (a) Cross-section; (b) Top-view; (c) Actual testing setup.

recording the potential difference via 100 Ω resistor $R_0$. The potential shifts were collected and recorded by a data collector - "Ultra low input current/Instrumentation amplifier/Analog to digital convertor, Demo 2011 CvB".

By these tests, the better understanding of the time-dependent process of stray current interference on steel (in stray current supplying period and after stray current supply period) can be obtained. These results will also be the supporting evidence of the corrosion product distribution (e.g., the relevance of the recorded back flow to the corrosion product nearby the cathode), observed by Environmental Scanning Electron Microscope (ESEM).

The measurement steps were as below:

Step 1 - Stray current supply stayed off, the OCPs of the specimens were recorded;

Step 2 - Turning on the external stray current supply for 250–300 s;

Step 3 - Cut-off of the stray current supply, then monitor the response after cut-off for 100–150 s.

Moreover, to investigate the effect of steel length on the level of stray current-induced corrosion, an additional layout was investigated as well: adding a third plain mortar cube between two specimens, to simulate longer length reinforced element undergoing stray current (i.e., a longer distance and additional resistance between anode and cathode). The schematics for this additional testing arrangement are shown in Fig. 5. In these tests the level of external stray current supply was 6 mA.

*2.2.4. Microstructural observation on corrosion product distribution*

At the end of test period (after all above tests), the distribution and morphology of the corrosion products formed at the steel-mortar interface were investigated using ESEM (the used equipment is ESEM Philips XL30), in a backscattered electrons (BSE) mode. The image analysis was performed at magnification 125x. The cross-sections of the steel-mortar interfaces for ESEM analysis were taken from identical geometrical locations of the cubes. Fig. 6 depicts the sampling strategy for ESEM analysis. For each specimen, 3 cross-sections were chosen: the cross-section at middle (namely "Middle") and 2 ends of the fully embedded steel piece (namely "End 1" and "End 2", respectively).

The cube was cut into 4 slices (Slices ①②③④, as shown in Fig. 6). Slice ② was used for cross-section "End 1", Slice ③ for "Middle", and Slice ④ for "End 2". These series of tests aimed to visually clarify the importance of rebar orientation on the level of stray current-induced corrosion, i.e., positioning and distribution of corrosion products on the steel surface, as influenced by the two different manners of rebar embedment in the cubes (see Fig. 2 and Fig. 6).

## 3. Results and discussion

### 3.1. OCP and $R_p$ evolution

The average OCP/$R_p$ values of 2 replicates per group are shown in Fig. 7. The OCP values for all specimens at 14 days of age are cathodic and far beyond the passivity threshold. This is due to the "fresh" mortar matrix (only 24 h fog room curing) [20]. After 102 days a more passive state is recorded for Cl-free cases. Additionally and with respect to positioning of the steel rebar in control (Cl-free) conditions, the following can be noted: specimens S(V) exhibit more anodic potentials (more noble). This is accompanied by higher $R_p$ values. In contrast, specimens S(P) present the relatively active state, judged from both OCP and $R_p$ values.

For the Cl-containing specimens, the OCP values of which remained negative. This is in line with the relatively low $R_p$ values (compared to the Cl-free situations), indicating the accelerated corrosion state in Cl-containing medium, and reflecting the coupling effect of stray current and $Cl^-$. At the end of conditioning (123 days), the most corrosive state is recorded for CS (P) specimens, exhibiting lower $R_p$ values and more cathodic OCP values than CS (V) specimens. It can be noted that the geometrical position of the steel affects the electrochemical response.
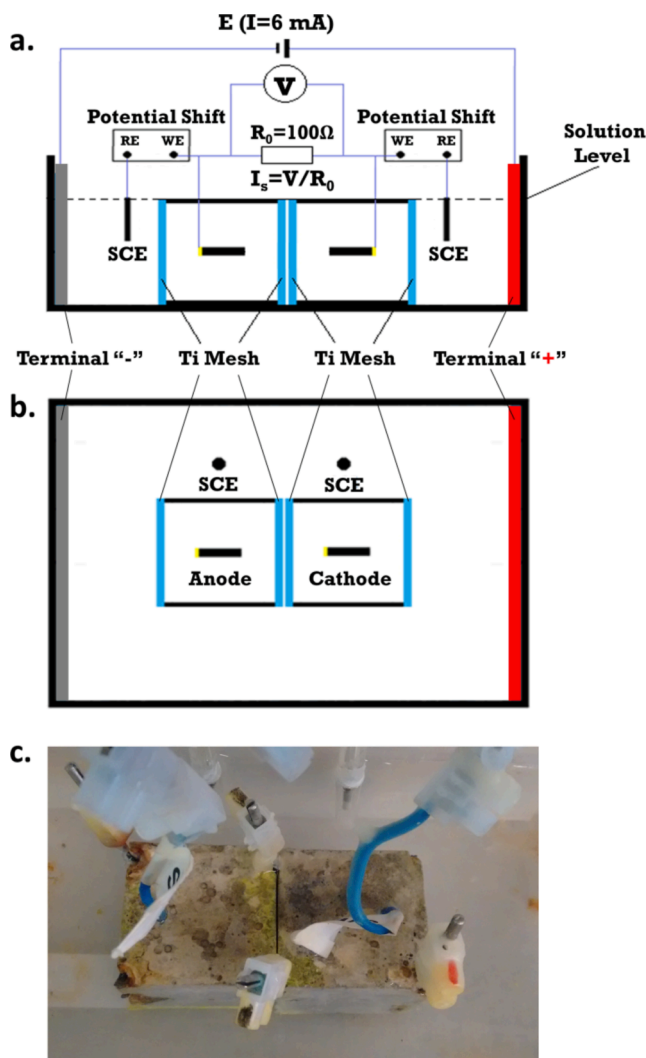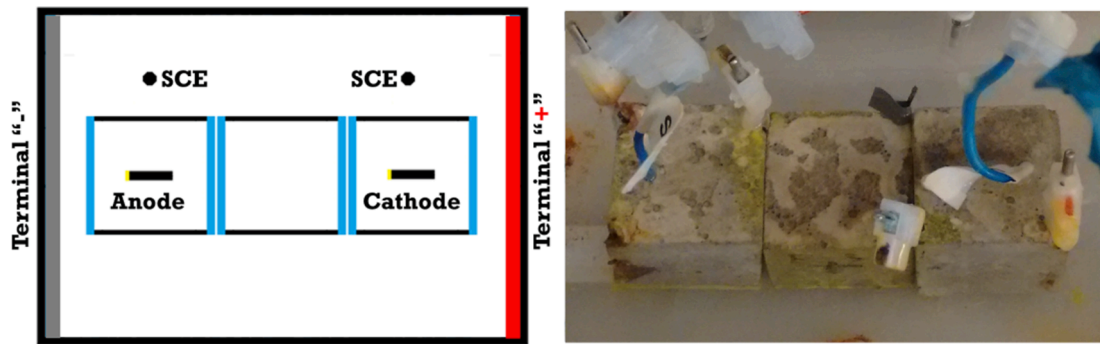
**Fig. 5.** Advanced testing arrangement for simulation of practical stray current electric field: longer length of steel undergoing stray current interference.
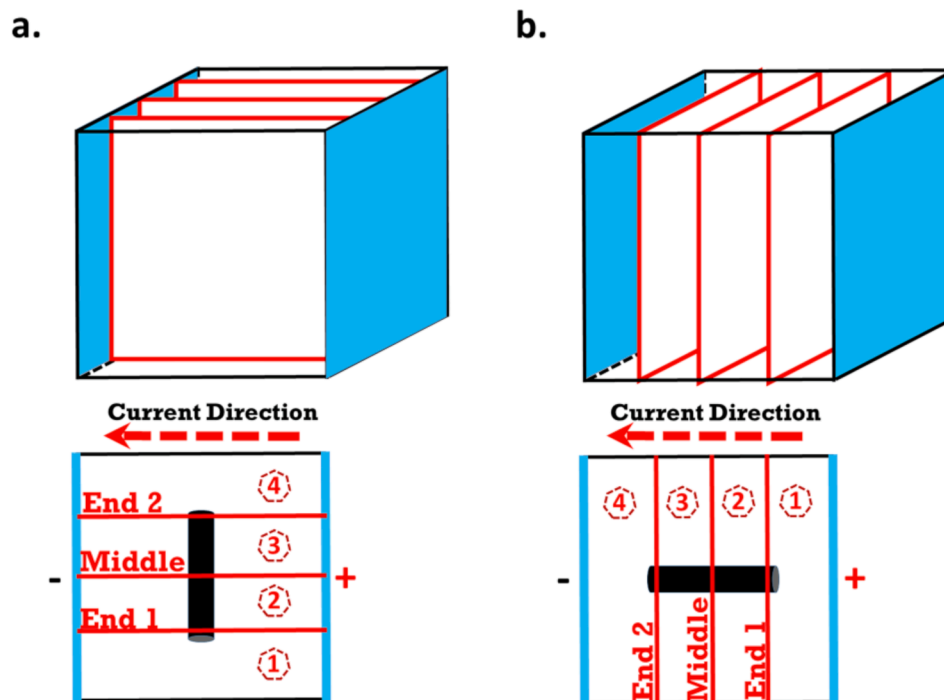


**Fig. 6.** Schematic and top-view of cross-sections for ESEM: (a) Steel bar vertical to the stray current direction; (b) Steel bar parallel to the stray current direction.
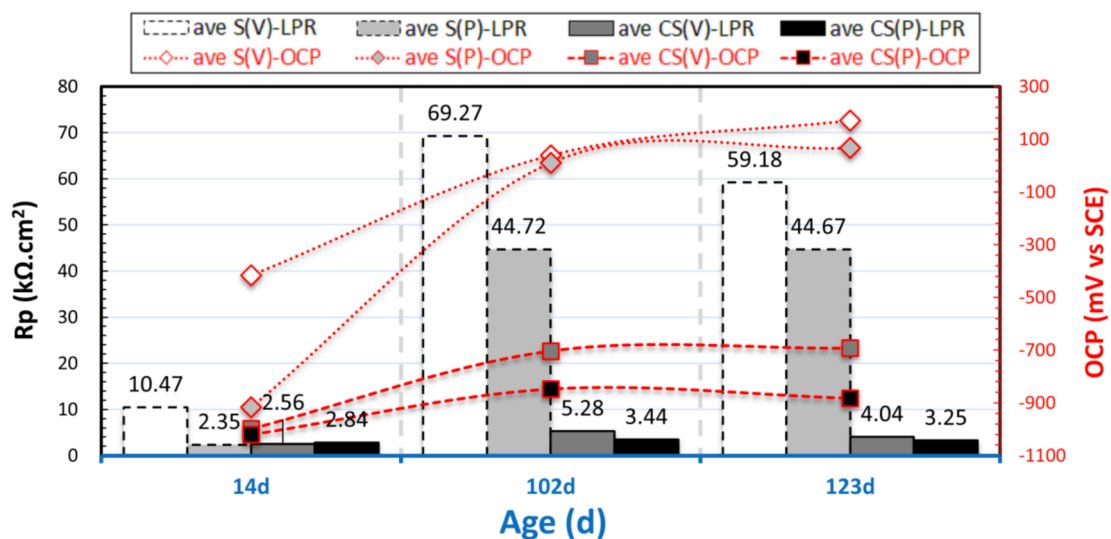


**Fig. 7.** Comparison of average OCP/ $R_p$ values of Cl-free groups: S(V) and S(P); and Cl-containing groups: CS(V) and CS(P).

The stray current interference is more significant for a steel bar parallel to the current direction, compared to the case of steel bar vertical to the current direction.

### 3.2. PDP and EIS

PDP results (at 123 days) are presented in Fig. 8a for the S-samples (in water), and in Fig. 8b for the CS-samples (in 5% NaCl). The EIS in Nyquist format of all samples at 123 days are shown in Fig. 9 and Fig. 10. According to the corrosion potential and anodic current density in Fig. 8, the corrosion resistance of the S(V) groups is higher than that for the S(P) groups. The highest anodic current density is recorded for S(P)-1 specimen. At around 0.42 V (vs SCE) of the PDP response for the S(P)-1 specimen, a current peak (about 15.92 $\mu A/cm^2$) is observed. This current maximum is related to the dissolution of product layer previously formed on the steel surface [21–23]. Similar behavior with an anodic current peak at +400 mV (vs SCE) is found for S(P)-2 specimen. An indication for dissolution of product layer (anodic current peak) is not observed for S(V)-1 and S(V)-2. This implies the lack of or a minimum amount of product layer on the steel surface of the S(V) cases.

The PDP responses of S(P)-1 and S(P)-2 specimens are in line with the EIS. A time constant at MF (middle frequency, between 120 Hz and 5 Hz) can be observed for S(P) cases - the |Z| value in MF of S(P)-1 is 3.6 Ω, which is higher than 2.2 Ω of S(P)-2. While this time constant is much

less pronounced for the S(V) specimens and shifted in frequency - see Fig. 9. This time constant at MF of S(P) EIS implies a thick, porous and non-homogeneous corrosion product layer in S(P) cases, denoting the pronounced corroding status of S(P) cases compared to S(V) specimens, which can be also reflected by the lower |Z| value in LF EIS response of S(P) cases. This, together with the anodic peaks of PDP, imply the more significant deposition and potential variations in the product layer properties/performance for S(P) cases.

According to the E/pH region (0.42 V vs SCE/pH≈13), it can be judged (based on the thermodynamic principles) that, the steel surface layer on specimens S(P)-1 and S(P)-2 is most likely Ca-substituted mixture of oxide and hydroxide or $Fe_2O_3 \cdot nH_2O$ [24]. Ca-containing product layer stabilizes the passive layer on the steel surface and further leads to a more uniform attraction and adherence of $Ca^{2+}$, resulting in a product layer with higher stability of S(P) groups [24]. Based on the PDP and EIS, it can be hypothesized that in the case of S(P) specimens a product layer of different amount, and/or distribution on the steel surface was formed. This is an indication of the more significant effect of stray current in S(P) groups, if compared to the S(V) groups (vertical direction of the rebar).

The anodic current of PDP response for the Cl-containing CS specimens (Fig. 8b) is one order higher than S groups (Cl-free), indicating the much more active status of CS specimens. This can also be reflected by the EIS LF responses of groups CS(V) and CS(P) (specimens immersed in
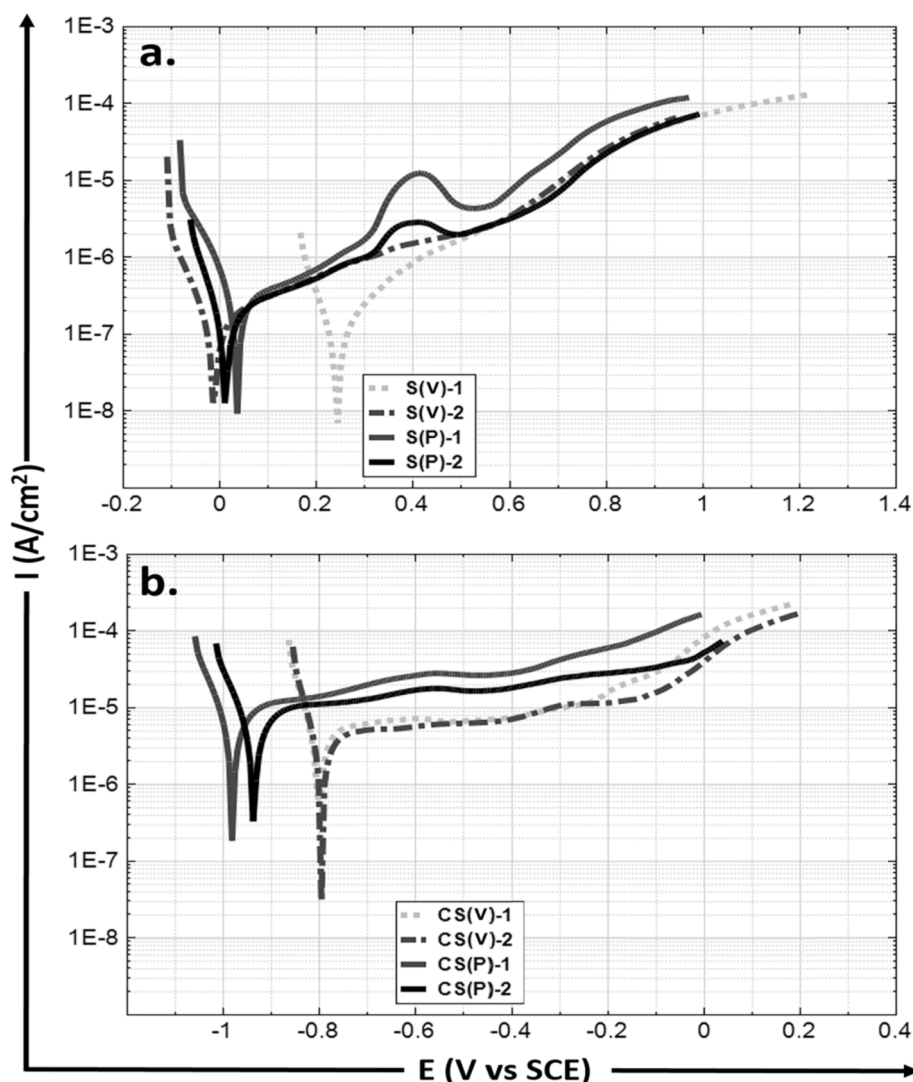


**Fig. 8.** Overlays of PDP response at 123 days, for: (a) Cl-free specimens; (b) Cl-containing specimens.
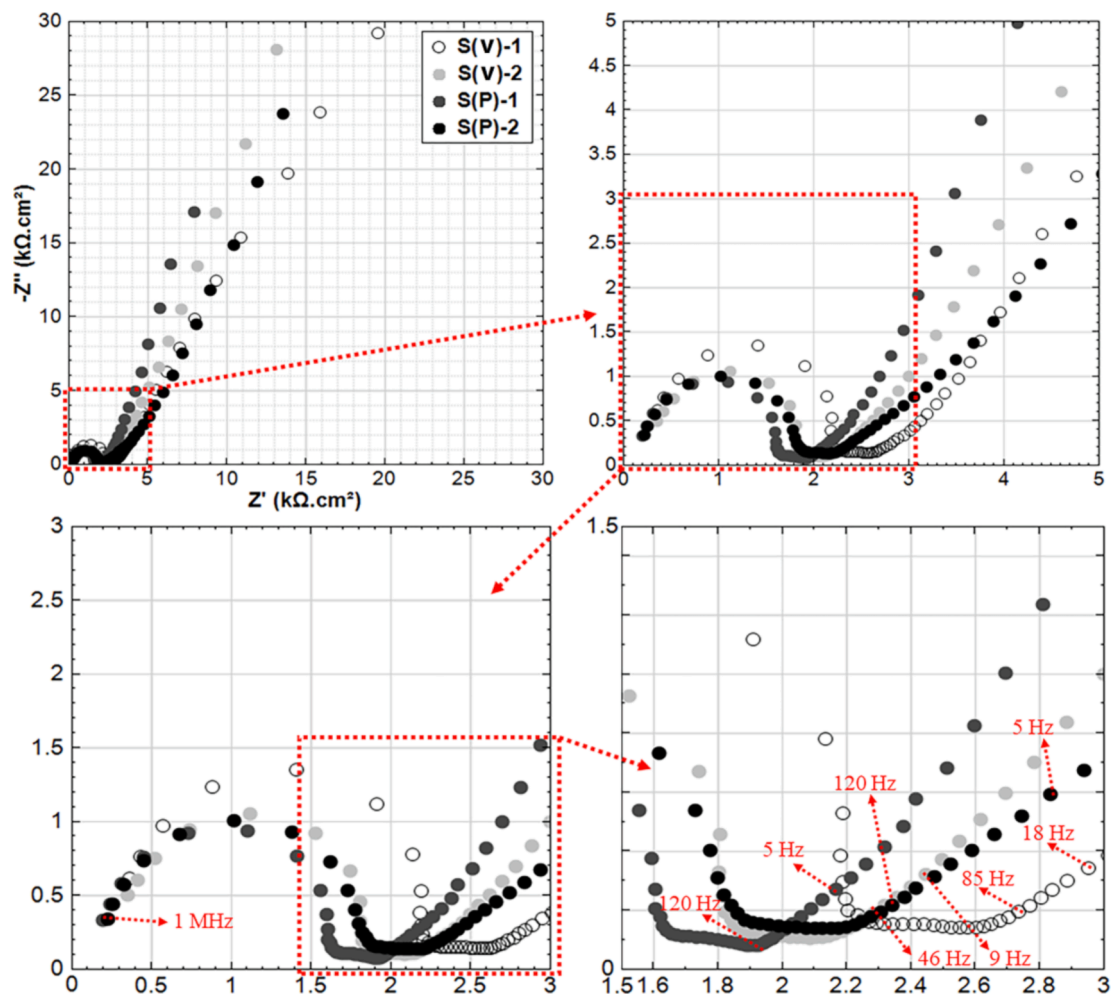
**Fig. 9.** Overlays of EIS response for Cl-free specimens at 123 days.

5% NaCl). The CS(P) specimens show higher anodic current compared to CS(V) cases. It can be judged from PDP, that the effect of stray current is more pronounced in the CS (P) group. Additionally, the small peaks in the CS(P) cases are recorded after −0.6 V (vs SCE) in the PDP (Fig. 8b). This points to a more significant accumulation of corrosion products on the steel surface of the specimens CS(P), compared to other cases.

Besides, there is also another observable difference between the CS (V) and CS(P) groups, judged from EIS tests. If the HF to MF response is compared in Fig. 10, we observe an additional time constant appears (between 5 and 0.2 Hz), especially pronounced for the CS(P) specimens. This time constant is linked to the abovementioned more pronounced accumulation of corrosion product over a larger surface of specimens CS (P). This time constant (between 5 and 0.2 Hz) is already in different frequency window compared to the control cases. These outcomes, together with the indication of PDP of the CS(P), again illustrate the larger stray current effects in the CS(P) groups, compared to CS(V) specimens. The above electrochemical behavior is well supported and visualised by ESEM observations at the steel-mortar interface, which will be discussed in Section 3.5.

### 3.3. Potential change monitoring on individual reinforced mortar specimens

At the age of 34 days, stray current was supplied on selected specimens, for about 1500 s, to monitor the potential change of the embedded steel undergoing stray current. These tests, as introduced in Section 2.2.2, were performed on vertical specimens S(V)-1 and S(V)-2. The test results in this section aim to justify the importance of the bulk matrix properties, on the level of current picked-up by the reinforcement. These specimens are meant to illustrate the stray current flowing paths, since the most significantly different performance is observed for S(V)-1 and S (V)-2, in both PDP tests (E$_{corr}$ values) and HF EIS (bulk matrix resistance), irrespective of the fact that S(V)-1 and S(V)-2 are replicates.

As can be seen in Fig. 11a, an anodic potential shift of S(V)-1 is recorded at the instant once the current supply is on - the potential increased immediately after the stray current application, from E$_{off2}$ = −140 mV, to the stable value of E$_{on}$ = 178 mV. This E$_{on}$ potential of 178 mV reflects the stray current-induced anodic polarization on the rebar. When the current is interrupted, a potential decay is recorded, reaching the value of −150 mV (E$_{off2}$). This value (E$_{off2}$) is similar to the initial E$_{off}$ of −140 mV, however, with 10 mV more cathodic. The anodic potential shift from E$_{off1}$ to E$_{on}$, together with the adopted more cathodic value of E$_{off2}$, compared to E$_{off1}$, imply a process of steel dissolution. Fundamentally, the driving force for steel corrosion is anodic polarization (the potential change from E$_{off1}$ to E$_{on}$ is an anodic shift) - this is the primary kinetic effect in steel corrosion.

Upon stray current interruption and prior to E$_{off2}$ stabilization (Fig. 11a), the potential-time curve includes the so-called ohmic drop (IR drop) component, equal to 271 mV for the S(V)-1 case. From this point forward (i.e. after the so-called instant-off potential E$_{ins.off}$ = −93 mV) a decay of 57 mV is observed. The IR drop contribution disappears in a very short time, normally in the order of 10$^{-6}$ s [25–27]. The potential decay (57 mV) means that indeed, the steel bar is polarized by the applied stray current, inducing an overall positive potential shift under
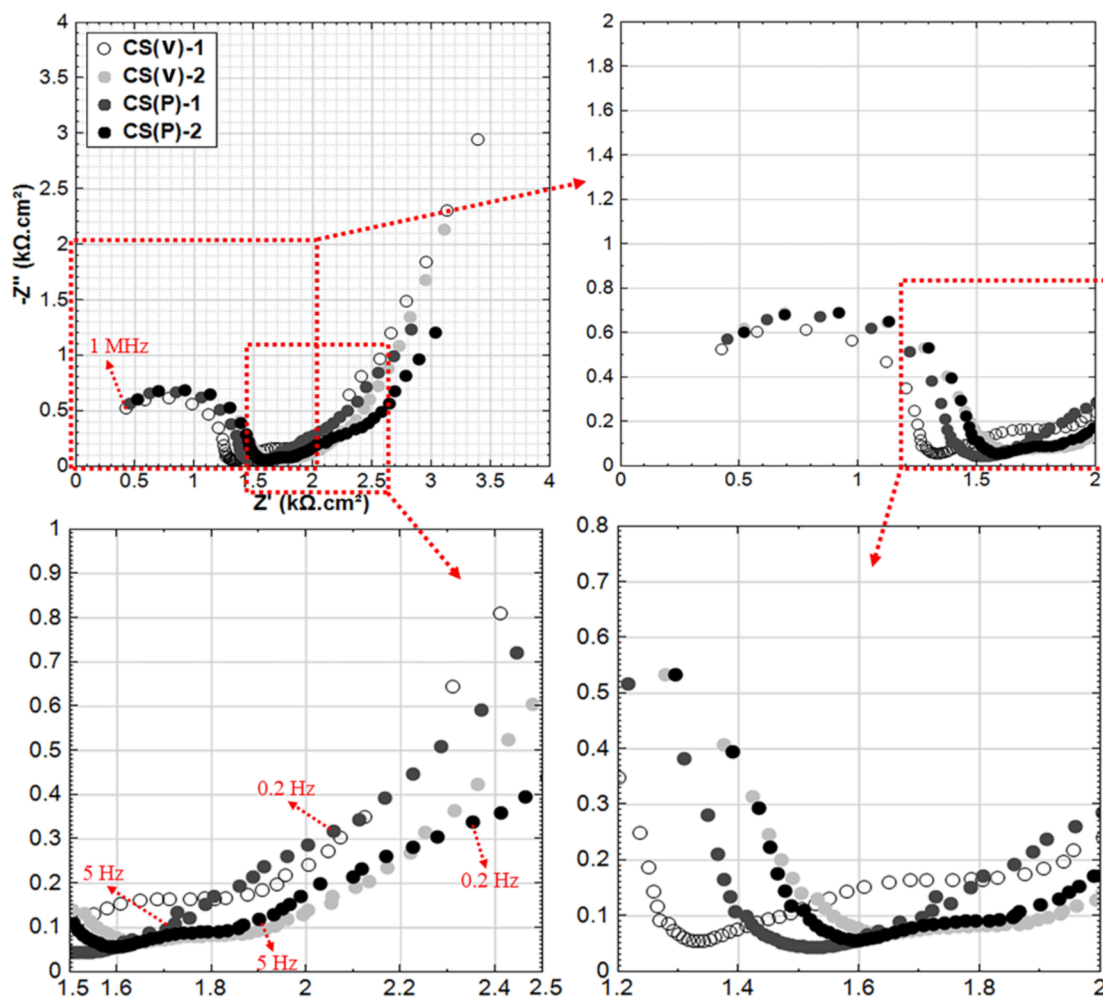
**Fig. 10.** Overlays of EIS response for Cl-containing specimens at 123 days.

current conditions. This means that in this situation, anodic polarization induced by stray current is a predominant phenomenon i.e. the stray current causes positive polarization, hence, enhances the driving force of steel corrosion following the principles of fundamental electrochemical kinetics.

A similar trend can be found for S(V)-2 (Fig. 11b): the IR drop of 217 mV and a potential decay of 125 mV can be observed after the shutdown of current supply. The lower IR drop of S(V)-2, compared to S (V)-1, reflects the lower resistance of mortar bulk matrix of S(V)-2. The higher potential decay of S(V)-2 implies the more efficient polarization of this rebar, undergoing the identical to S(V)-1 stray current supply. This again reflects the lower resistance of the mortar bulk matrix of S(V)-2, because if the lower resistance of bulk matrix (compared to S (V)-1) was at hand, the stray current can flow into the steel more easily. The sequence of this is the more significant corrosion of S(V)-2.

The lower bulk matrix resistance of S(V)-2 is in accordance with the lower impedance of EIS HF response (Fig. 9), as already discussed is Section 3.2. The lower corrosion resistance of S(V)-2 can also be verified by the PDP (Fig. 8): the corrosion potential of S(V)-1 is 200 mV more noble than S(V)-2, corrosion current for S(V)-2 is higher. A gradual increase of anodic current with PDP polarization after corrosion potential is recorded for S(V)-1, while there is anodic limitation for S(V)-2. This means that a less significant corrosion product accumulation is relevant for S(V)-1, compared to S(V)-2.

### 3.4. Mechanism of stray current-induced corrosion initiation with respect to geometrical layout of the bar

Based on the above results, it can be concluded firstly that, the stray current interference is more pronounced for a steel bar parallel to the current direction than the case of steel bar vertical to the current direction. In the former case, parallel position, the effect of stray current is significant, since the full length of the bar is exposed to the field of stray current flow, i.e., the portion of stray current "picked-up" by the bar flows through the full length of rebar, since the bar is the least resistive path. However, for the vertical case, the effect of stray current is limited to the cross section of the bar only.

The stray current ($I_s$) inducing reinforcement corrosion in a reinforced concrete element, and the schematics of stray current parallel or vertical to steel rebar are shown in Fig. 12. In this case, stray current originates from the positive terminal of a foreign DC electrical source, and flows to an alternative path (underground reinforced concrete element) through the soil and concrete cover. Due to the low resistivity of the steel rebar, if compared to the surrounding concrete, the stray current can easily be picked-up by the embedded reinforcement.

The stray current would flow along the reinforcement between cathodic and anodic areas, where the ohmic drop ($\psi_\Omega$ in Fig. 12) would also be present. An anodic reaction (metal dissolution) will occur where the stray current flows out (is discharged) from the reinforcement (anodic area). At this location, anodic polarization induced by the current outflow ($\psi_a$ in Fig. 12) will be relevant. This means that the process of (stray current-induced) steel corrosion is initiated and accelerated at
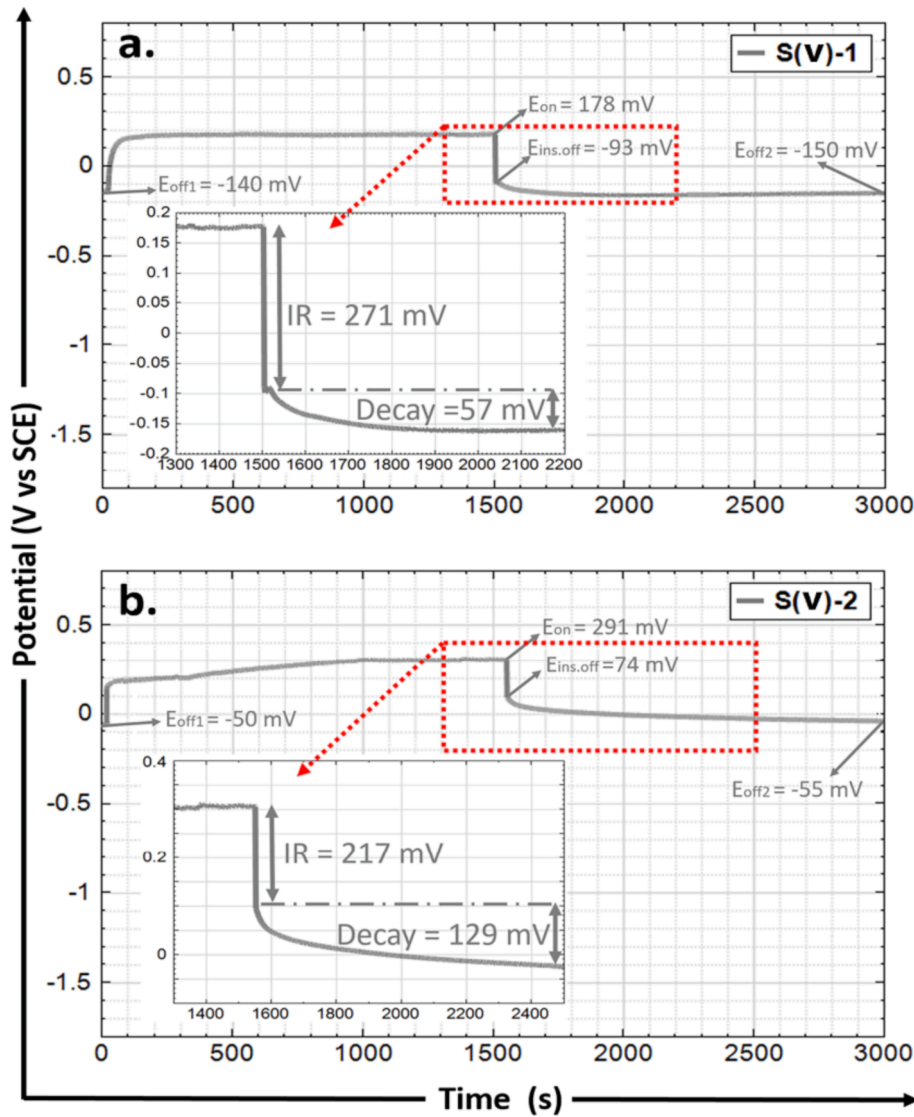
**Fig. 11.** Monitoring of potential shift undergoing stray current: (a) S(V)-1; (b) S(V)-2. (specimen and reference electrode arrangement for potential shift monitoring in Fig. 3).

this location. The current outflow would return to the negative terminal of the foreign DC source, "passing" through the concrete cover and soil, and closing the electrical circuit.

If stray current can be "picked-up" by the steel reinforcement, a driving voltage ($\Delta U$, see Fig. 12) has to be present [1,8]:

$$\Delta U = \psi_c + \psi_a + \psi_\Omega \tag{1}$$

This voltage equals the sum of cathodic ($\psi_c$) and anodic ($\psi_a$) polarizations, in case the ohmic drop ($\psi_\Omega$) through the reinforcement is negligible because of the low resistivity of the steel rebar:

$$\Delta U = \psi_c + \psi_a \tag{2}$$

This driving voltage ($\Delta U$) is the potential difference (produced by supplied stray current surrounding the steel rebar) between the cathodic and anodic polarized regions, equals to $L \bullet \lambda \bullet I$: $\Delta U = L \bullet \lambda \bullet I$, where, $L$ is length of anodic and cathodic sites of steel undergoing stray current; $\lambda$ is resistance of mortar matrix per unit length; $I$ is stray current flowing in mortar matrix. If stray current can be picked-up by steel, $\Delta U$ must be higher than the sum of the cathodic ($\psi_c$) and anodic ($\psi_a$) polarizations induced by inflow and outflow of stray current circulating in the steel, i. e., $L \bullet \lambda \bullet I > \psi_c + \psi_a$. The higher $L$, the higher driving voltage ($\Delta U$) is present and the easier stray current can be picked-up by steel - and vice

versa.

Besides inducing corrosion, stray current can also result in the different distribution of corrosion products. Stray current produces the variation of distribution of anodic and cathodic sites (with a distance of $L$) on steel surface. For the parallel situation (Fig. 12a), the $L$ (length of steel conducting the current) is longer than vertical situation (Fig. 12b), i.e., in the parallel situation the distance of anodic and cathodic regions is longer than that in vertical situation. In the parallel case, with long distance between the anode and cathode, stray current induces a macrocell-like corrosion. Corrosion products do not accumulate at the exact anodes where current flows out, but nearby the anodic sites. For the vertical case with shorter distance between the anode and cathode, a microcell-like corrosion mechanism is relevant, where many microcells will finally result in a corrosion damage at this particular cross section. In both situations and as a next step, the accumulated corrosion products occupy the steel-bulk matrix interface and further can penetrate into the bulk matrix. In parallel situation, the localized corrosion products can more easily penetrate into the bulk matrix compared to uniform corrosion, and further more intensively deteriorate the steel-concrete interface and decrease the bond strength of steel-concrete interface. The propagation of corrosion product into the mortar matrix is observed by ESEM, and will be discussed in the next section.
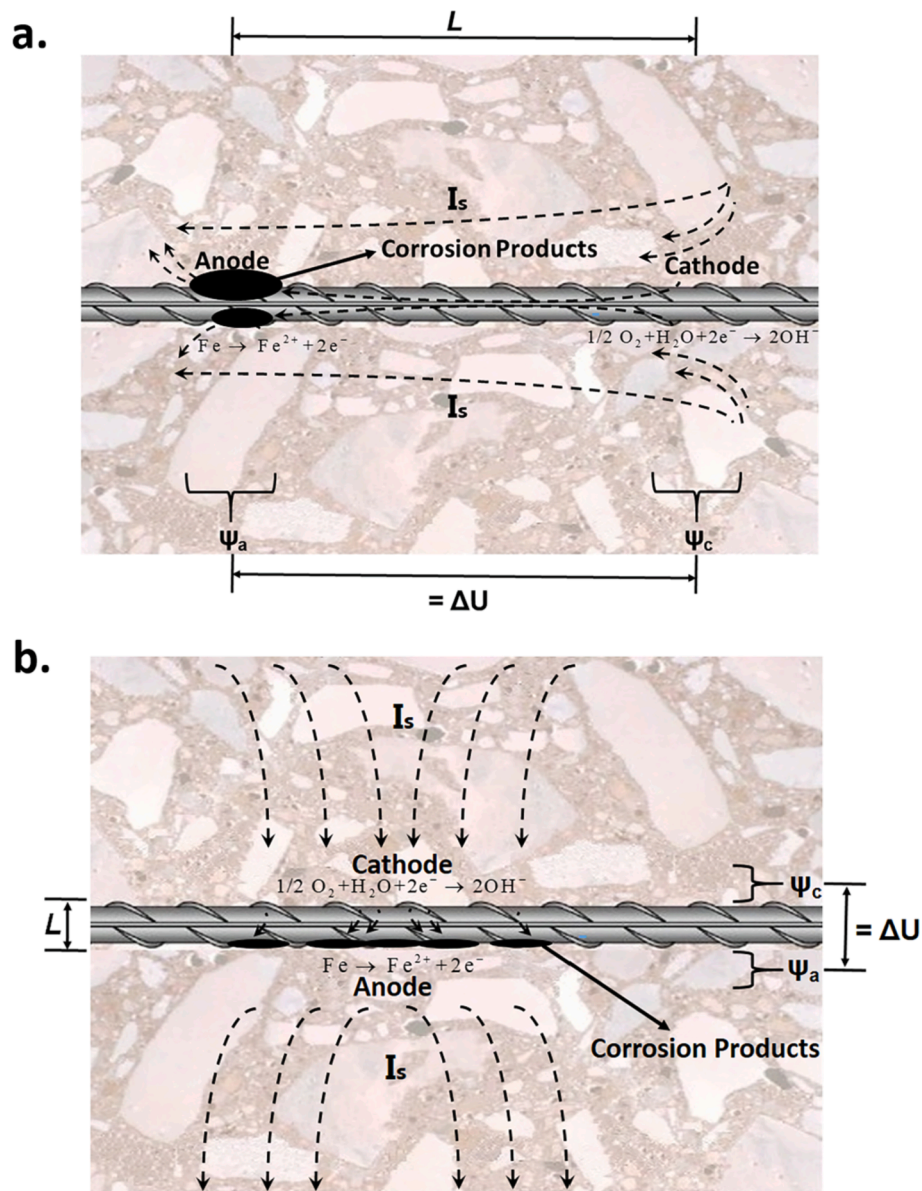
**Fig. 12.** (a) Schematic of stray current parallel to steel rebar: Macrocell-like, tends to induce localized corrosion; (b) Schematic of stray current vertical to steel rebar: Microcell-like, tends to induce general/uniform corrosion.

*3.5. ESEM observation*

The combination of ESEM observations and the obtained electrochemical parameters reflect the distribution of corrosion product on the steel surface. Hence a better insight into the mechanisms of stray current corrosion can be achieved. To this aim, the ESEM observations were performed on only corroding cases, where the corrosion products are more pronounced and visible than in the control cases.

The ESEM images taken at different locations of "End 1" and "Middle" cross-sections of CS(V)-1 are shown in Fig. 13. The images of "End 1" and "End 2" cross-sections of CS(P)-2 are shown in Fig. 14. The location of each cross-section of specimen is also illustrated in the inlet of according figures.

These series of images aim to visualise the effects of rebar direction, on distribution of corrosion product along radial direction: CS(V)-1 for steel rebar vertical to stray current, and longitudinal direction: CS(P)-2 for steel rebar parallel to stray current. For instance, the anode is expected to be mostly corroded (because of current outflow), the corrosion product may be localized at the anodic site, which is determined by the direction of stray current.

As can be seen in Fig. 13, the "anode" and "cathode" coexist in both cross-sections of CS(V)-1 according to the direction of stray current flow. In this situation the anode and cathode are close by (distance between them is just the rebar diameter 6 mm). For CS(P)-2 as indicated in Fig. 14, the "anode" is the whole "End 2" cross-section, "cathode" is the whole "End 1" cross-section. The distance between anode and cathode is the length of rebar (2 cm).

As can be seen in Fig. 13a, more corrosion product is accumulated on the "anode" side (see Plot 4, 5, 6 in Fig. 13a) of the "End 1" cross-section of CS(V)-1. Similar trend is observed in Fig. 13b - the most severe corrosion is observed at the "anode" side (see Plot 5, 6, 7 in Fig. 13b) of the "Middle" cross-section of CS(V)-1. This is obviously attributed to the stray current direction.

It can be noted that the corrosion product is also formed at the "cathode" location (Plot 2 in Fig. 13) in both cross-sections of CS(V)-1. However, the corrosion damage at the "cathode" side is visually much less than that at the "anode" side. The corrosion at "cathode" here is attributed to Cl$^-$ in the vicinity of steel surface. Another cause for the
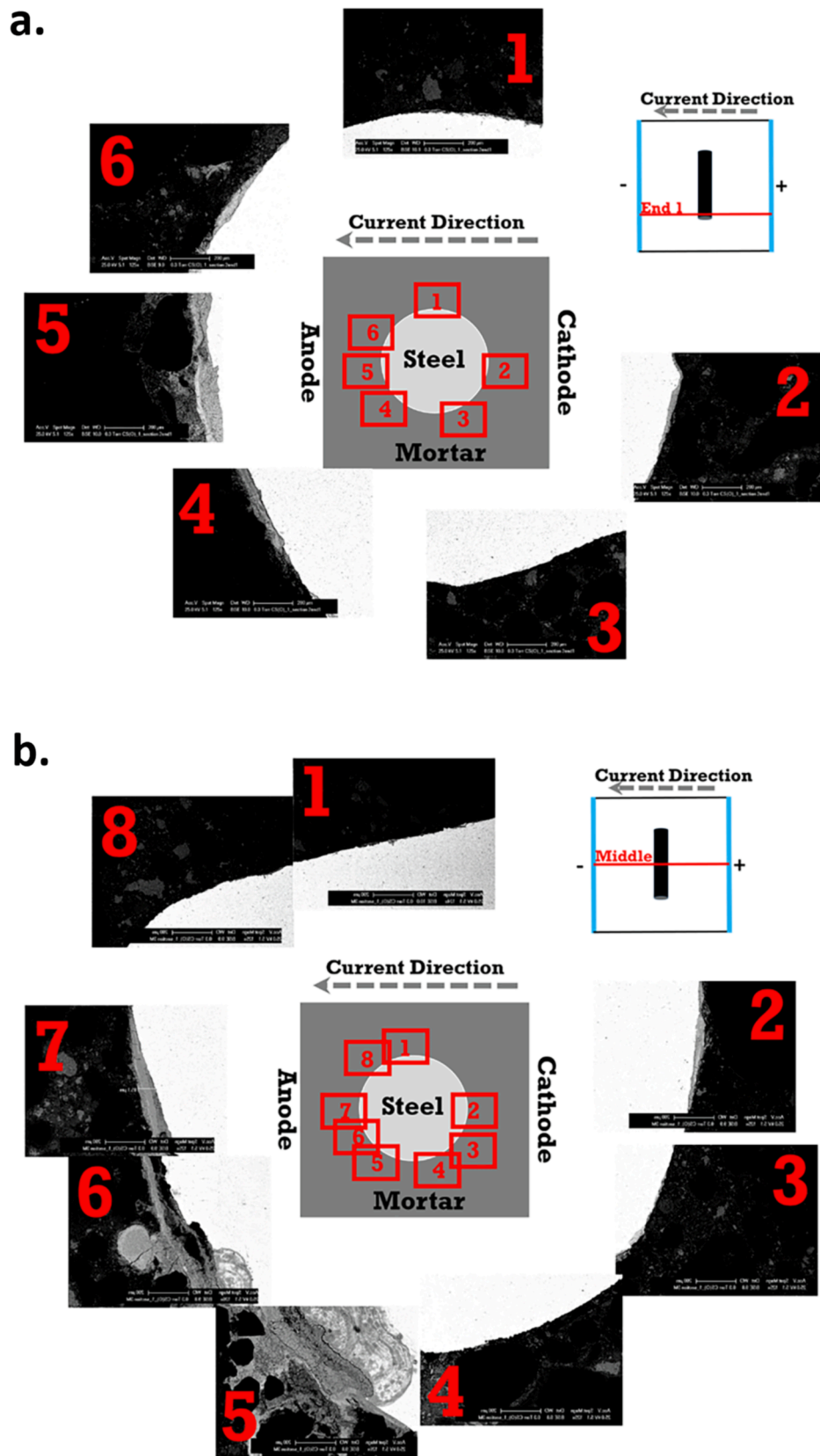
**Fig. 13.** ESEM images (BSE mode) at different locations of the steel-mortar interface: (a) the "End 1" cross-section of CS(V)-1; (b) the "Middle" cross-section of CS (V)-1.
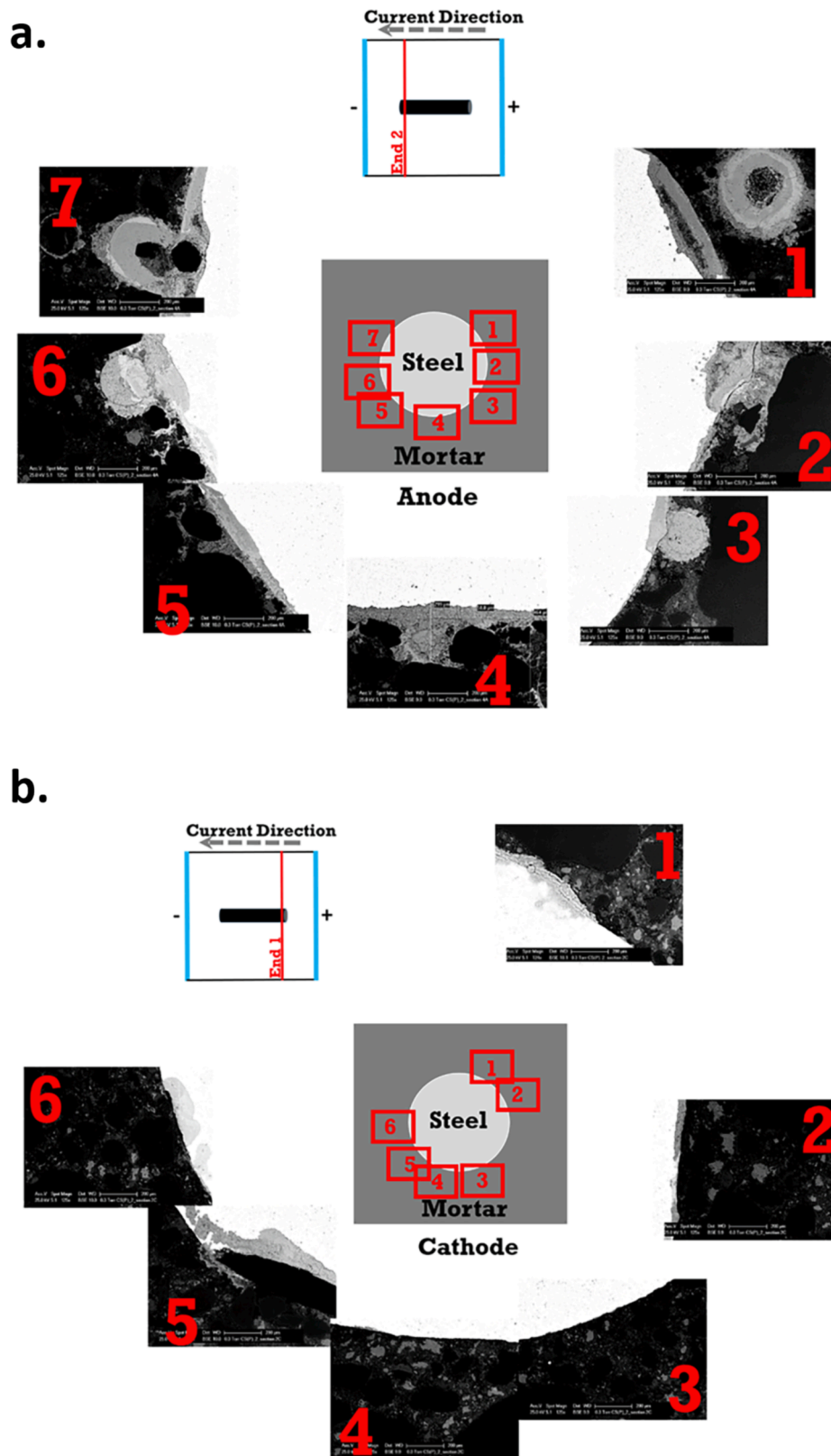
**Fig. 14.** ESEM images (BSE mode) at different locations of the steel-mortar interface: (a) the "End 2/Anode" cross-section of CS(P)-2; (b) the "End 1/Cathode" cross-section of CS(P)-2.

corrosion at "cathode" is the back flow of current once the stray current is switched off. The back flow is induced by the potential difference between anode and cathode when the stray current supply is on. Once the stray current is cut off, a reversed current will flow from "anode" to "cathode". This back flow is actually recorded and will be discussed in the next Section 3.6.

As for the cross-sections of CS(P)-2, much more corrosion product is observed at the "anode" location (Fig. 14a), i.e., "End 2" cross-section

(compare to "cathode" - "End 1" cross-section in Fig. 13b). It is obvious that the corrosion accumulation at the "anode" of CS(P)-2 is more intensive than the "anode" of CS(V)-1. As can be observed in Fig. 14a in some locations of "anode" of CS(P)-2 ("End 2" cross-section), the corrosion product even penetrates into the surrounding mortar matrix (Plots 1, 3, 6, 7 in Fig. 14a). This verifies the hypothesis proposed in section 3.4: stray current parallel to steel rebar leads to localized corrosion more easily.

For the "cathode" of CS(P)-2 ("End 1" cross-section), the corrosion product is only observed at Plots 1, 2, 5, 6 (see Fig. 14b). The substantial penetration of corrosion product into the mortar matrix is not observed in "cathode" cross-section. This may be because the cathode is far away from the anode. Hence there is more resistance to the back flow towards the cathode in this situation. All these observations again indicate the effect of steel rebar layout on distribution of corrosion product induced by stray current: the rebar parallel to stray current leads to more significant corrosion than rebar vertical to stray current.

### 3.6. Picked-up current monitoring

As aforementioned, the aim of these tests (as introduced in Section 2.2.3) was to monitor the picked-up stray current level. The stray current electrical field was simulated in 5% NaCl medium (as external environment). The obtained test results are the supporting evidence of the corrosion product distribution (for example, due to the recorded back flow), observed by ESEM.

As shown in Fig. 15a, the current level picked-up by steel is around 0.01 mA of the peak value. In this simulated stray current electrical field, it is clear that only small part of the supplied stray current can flow into the steel rebar. The IR drops are clearly recorded instantaneously after application and cutting off of the current. At the instant when the stray current is applied, i.e., at the "ON" point as arrow-indicated in Fig. 15a, it is clear that CS(P)-1 is the cathode and CS(P)-2 the anode, according to the negative potential shift for steel piece CS(P)-1 and positive for CS(P)-2.

This trend can also be judged by the constant direction of current flowing within the steel pieces (i.e., the negative sign of current): the current flows into CS(P)-1 firstly (cathodic current), flows through the shunt resistor $R_0$, and finally flows out (anodic current) at the steel piece of CS(P)-2. In the present work, the sign of the current is defined as the current direction: the negative sign means the current flowing from CS(P)-1 to CS(P)-2, while the positive values of current show the
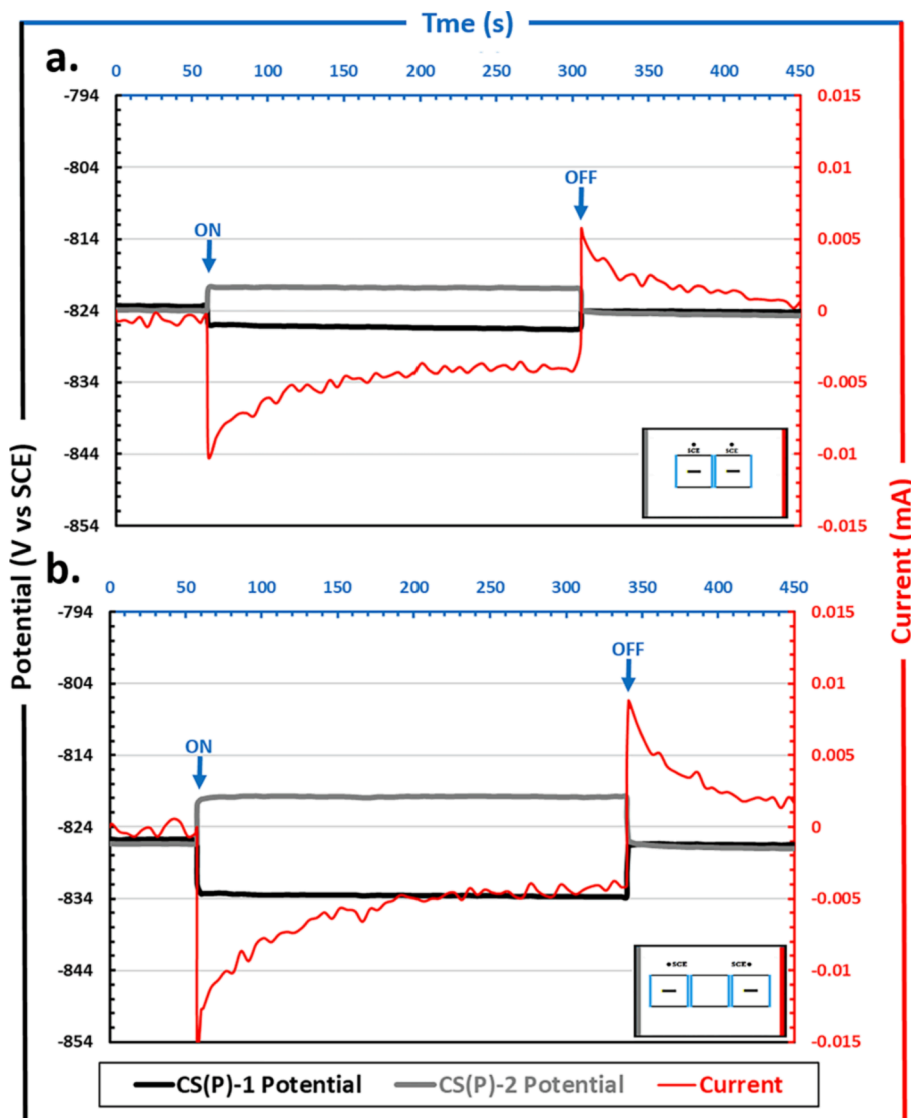


**Fig. 15.** Response of CS(P)-1/CS(P)-2 undergoing simulated practical stray current electric field (6 mA) in Cl⁻ containing environment: (a) basic arrangement (test arrangement in Fig. 4, performed after 123d); (b) advanced arrangement, longer length of steel undergoing stray current (test arrangement in Fig. 5, performed after 123 d).

opposite direction of current flow.

What can clearly be observed is that the stray current flowing into the steel rebar is decreasing. As can be seen in Fig. 15a, after the current is just supplied (i.e., after the "ON" point), the measured current level sharply changes from zero to around −0.01 mA, thereafter decreases. This observation can be attributed to the coexistence of polarization resistance and double layer capacitance on the steel-mortar interface (i. e., a typical Randles circuit). The transient response of steel surface induced by a given electrical interference is governed by the property of this Randles circuit [27].

Upon applying the stray current electrical field, part of current is picked-up by the steel. The picked-up current flowing in steel contains two components in parallel: part of it is "Non-faradic current", which can only play role on charging the double layer capacitance (for CS(P)-1 is charging, while for CS(P)-2 is discharging when current is just "ON" as shown in Fig. 15a); simultaneously the other part of current takes part in the redox reactions (CS(P)-1 is reduction due to cathodic current, while CS(P)-2 is oxidation because of anodic current), which is the so-called "Faradic current" [28–32]. Once the double layer capacitor is fully charged, only the "Faradic current" can circulate within the steel. This is the reason why the picked-up current is decreasing.

At the instant of t = 300 s (see Fig. 15a), when the stray current supply is turned off, a sudden positive increase of current flowing within steel pieces is monitored (i.e., back flow), again followed by the decrease of current level. This abrupt alternation of negative to positive sign of the picked-up current, implies a direction change of the current flowing within the steel pieces. This is attributed to the potential difference between cathode and anode, previously induced by inflow and outflow of stray current. This recorded back flow is the supporting evidence of the corrosion product distribution, i.e., the relevance of back flow to corrosion product nearby the cathode. To build the current loop, the back flow will then circulate within the concrete matrix between anode and cathode. Hence the back flow will be influenced by the concrete resistance according to the Ohm's law: the higher the resistance value of concrete, the lower the value of back flow, and vice versa.

As already introduced, the longer distance between 2 pieces of steel bars (i.e., anode and cathode) was produced (another non-reinforced cube was placed between CS(P)-1 and CS(P)-2, see Fig. 5). It can be observed in Fig. 15b that similar trends/shapes of time-dependent response are recorded. However, this "3 cubes case" shows the higher values for the level of picked-up current and higher potential shift. In other words, the response of "3 cubes case" is more intensive than the "basic arrangement". In the "3 cubes case", the resistance of the bulk matrix between anode and cathode is higher. This case shows more significant "Macrocell-like" behavior, and undergoes more intensive polarization (resistance polarization). The consequence of the above is the higher stray current interference on steel surface. This implies that, for practical reinforced concrete structure, once the contacts of steel bars (between main reinforcement and stirrup) are loose, the stray current corrosion will be more severe at the anodic locations. In this situation the resistance between steel bars is higher, and the macrocell is more easily to be produced by stray current, hence the polarization effects induced by stray current are more significant.

As can be observed in Fig. 15b, a potential difference between the 2 steel bars has been established at the time interval of 50–340 s, which is due to the stray current interference: CS(P)-1 is cathode, and cathodically polarized because of current inflow; however CS(P)-2 is anode, anodically polarized due to the current outflow. At the instant when the stray current is just absent, the induced potential difference between anode and cathode still exists (at 340 s). This induced potential difference leads to an opposite current flow from the previous anode to the previous cathode.

In other words, the spontaneous interconversion between anode and cathode occurs just after the instant as the stray current is cut off. This means that in case of stray current-induced corrosion, corrosion (anodic reaction, i.e., the steel dissolution) can not only occur at the location

(the anode) where picked-up current flows out when stray current is present, but also on the position where stray current flows into the steel (previous cathode, but transformed to anode) when stray current is just off. This is actually observed by ESEM. If insulation on reinforced elements is adopted (a coating for example) to mitigate the stray current corrosion, not only the area of the anode portion induced by stray current should be insulated, but also the location nearby the anode, to prevent the back flow around the anode portion after the stray current attack. In fact, a best case scenario would be to insulate the full length of the conductive path (both anode and cathode). This aims to absolutely cut off the stray current picking-up and leaving paths.

### 3.7. Summary of effects of steel rebar layout on stray current-induced corrosion

In summary, compared to the situation of a steel bar vertical to the current direction, the more significant corrosion states are recorded when the steel bar is parallel to current direction. Stray current parallel to steel rebar tends to induce localized corrosion, in contrast the vertical situation leads to relatively uniform corrosion on the affected area. At the instant that the stray current supply is turned off, an opposite current flow (back flow) from the previous anode to the previous cathode is recorded. According to these results, some recommendations for the related challenges in civil engineering practice are as below:

To evaluate the stray current corrosion possibility, the reinforced concrete element parallel to stray current should be firstly inspected. Sectionalization of reinforced concrete structures (similar to the principle of general expansion joint in civil engineering) is a possible solution for reducing the stray current effect, as it is found that the longer length of steel rebar leads to more severe corrosion damage. The sectionalized structure means shorter length of reinforced elements undergoing stray current.

For modeling or predicting the bond properties of steel-concrete interface undergoing stray current, the corrosion product distribution should be considered as well. In this aspect the post-stray current effect, for instance the back flow, should be involved, as the back flow redistributes the corrosion product after the stray current interference.

### 4. Conclusions

The main objective of this work is to investigate the role of the rebar layout in conditions when stray current induces corrosion damage. The vertical and parallel directions (to stray current) of the cast-in steel are investigated in different conditions. Additionally, for clarifying the time-dependent response of steel rebar undergoing stray current, the potential shift and current level of stray current picked-up by steel are studied in a variety of layouts. The recorded time-dependent response can be the foundation for interpreting the data obtained from practical stray current monitoring. Besides an expansion of the database for monitoring stray current interference on reinforced concrete structures, the recorded results can be the basis for better understanding the process of stray current interference.

Based on the testing results, the related conclusions are listed:

The geometrical position of the steel bar undergoing stray current affects the electrochemical response and polarization intensity of steel rebar induced by stray current. Compared to the situation of a steel bar vertical to the current direction, a more significant corrosion state is recorded when the steel bar is parallel to current direction.

The "anode" and "cathode" areas are distinguished in each cross-section of the steel-mortar interface underwent stray current. Stray current parallel to the steel rebar tends to induce localized corrosion, in contrast the vertical situation, where a relatively uniform corrosion of the relevant section is at hand. A more significant corrosion product accumulation and deeper corrosion penetration are

observed on a steel rebar parallel to stray current, nearby the locations where the current leaves the steel rebar.

Though the supplying stray current is constant, the level of current picked-up by the steel rebar is decreasing. This observation can be attributed to the coexistence of polarization resistance and double layer capacitance on the steel-mortar interface.

At the instant when the stray current supply is turned off, an opposite current flow (back flow) from the previous anode to the previous cathode is monitored. It is attributed to the stray current-induced potential difference between the anode and cathode. This implies the spontaneous interconversion between anode and cathode induced by stray current, i.e., post-stray current effect. Thus not only the anodic part of steel, but also the temporary cathodic portion should be carefully considered and treated.

*CRediT authorship contribution statement*

**Zhipei Chen:** Conceptualization, Methodology, Investigation, Writing – original draft, Writing – review & editing, Visualization. **Liang Gao:** Methodology, Writing – review & editing, Project administration, Supervision. **Dessi A. Koleva:** Methodology, Writing – review & editing, Project administration, Supervision.

## Declaration of Competing Interest

The authors declare that they have no known competing financial interests or personal relationships that could have appeared to influence the work reported in this paper.

## Acknowledgments

## References

[1] Z. Chen, D. Koleva, K. van Breugel, A review on stray current-induced steel corrosion in infrastructure, Corros. Rev. 35 (2017) 397–423.

[2] L. Bertolini, M. Carsana, P. Pedeferri, Corrosion behaviour of steel in concrete in the presence of stray current, Corros. Sci. 49 (2007) 1056–1068.

[3] I. Lingvay, A. Voina, C. Lingvay, C. Mateescu, The impact of the electromagnetic pollution of the environment on the complex build-up media, Rev. Roum. Sci. Techn. Series Electrotech. Energ. 53 (2008) 95–112.

[4] D.K. Kim, T.H. Ha, Y.C. Ha, J.H. Bae, H.G. Lee, D. Gopi, J.D. Scantlebury, Alternating current induced corrosion, Corros. Eng., Sci. Technol. 39 (2004) 117–123.

[5] R. Dodds, DC traction stray current control - A case study from a utility, IEE Colloq. (Digest) (1999) 49–52.

[6] Z. Chen, D.A. Koleva, K. van Breugel, Electrochemical Tests in Reinforced Mortar Undergoing Stray Current-Induced Corrosion, in: L.E. Rendon Diaz Miron, D.A. Koleva (Eds.) Concrete Durability: Cementitious Materials and Reinforced Concrete Properties, Behavior and Corrosion Resistance, Springer International Publishing, Cham, 2017, pp. 83–108.

[7] A. Demetriou, D. Buxton, C.A. Charalambous, Stray Current DC Corrosion Blind Spots Inherent to Large PV Systems Fault Detection Mechanisms: Elaboration of a Novel Concept, IEEE Trans. Power. Delivery 33 (2018) 3–11.

[8] A.O.S. Solgaard, M. Carsana, M.R. Geiker, A. Küter, L. Bertolini, Experimental observations of stray current effects on steel fibres embedded in mortar, Corros. Sci. 74 (2013) 1–12.

[9] S.J. Duranceau, W.J. Johnson, R.J. Pfeiffer-Wilder, A Study Examining the Effect of Stray Current on the Integrity of Continuous and Discontinuous Reinforcing Bars, Exp. Tech. 35 (2011) 53–58.

[10] Z. Chen, D.A. Koleva, E. Schlangen, Bond of steel-mortar interface interfered by stray current, Cem. Concr. Res. 150 (2021) 106591.

[11] ZhiGuang Chen, ChaoKui Qin, JiXu Tang, Y. Zhou, Experiment research of dynamic stray current interference on buried gas pipeline from urban rail transit, J. Nat. Gas. Sci. Eng. 15 (2013) 76–81.

[12] S. Spagnuolo, A. Meda, Z. Rinaldi, A. Nanni, Precast concrete tunnel segments with GFRP reinforcement, J. Composite Constr. 21 (2017).

[13] A.M. Kerimov, P.A. Spirin, R.A. Kerimov, Relationship between the parameters of stray current circuits and the traction load, Prot. Met. 42 (2006) 409–411.

[14] Y. Luo, C. Wang, C. Luo, Q. Huang, S. Wang, X. Peng, Effect of electrical field on TSA failure of cement-based materials, Cem. Concr. Res. 90 (2016) 19–26.

[15] A. Susanto, D.A. Koleva, K.V. Breugel, The effect of water-to-cement ratio and curing on material properties of mortar specimens in stray current conditions, J. Adv. Concr. Technol. 15 (2017) 627–643.

[16] C.A. Charalambous, P. Aylott, D. Buxton, Stray Current Calculation and Monitoring in DC Mass-Transit Systems: Interpreting Calculations for Real-Life Conditions and Determining Appropriate Safety Margins, IEEE Veh. Technol. Mag. 11 (2016) 24–31.

[17] S. Xu, W. Li, F. Xing, Y. Wang, R. Wang, X. Wang, An elimination method of temperature-induced linear birefringence in a stray current sensor, Sensors 17 (2017).

[18] S.R. Allahkaram, M. Isakhani-Zakaria, M. Derakhshani, M. Samadian, H. Sharifi-Rasaey, A. Razmjoo, Investigation on corrosion rate and a novel corrosion criterion for gas pipelines affected by dynamic stray current, J. Nat. Gas. Sci. Eng. 26 (2015) 453–460.

[19] L.I. Freiman, Stray-Current Corrosion Criteria for Underground Steel Pipelines, Prot. Met. 39 (2003) 172–176.

[20] Z. Chen, D. Koleva, Corrosion Behavior of Reinforcing Steel Undergoing Stray Current and Anodic Polarization, Materials 14 (2021) 261.

[21] E. Volpi, A. Olietti, M. Stefanoni, S.P. Trasatti, Electrochemical characterization of mild steel in alkaline solutions simulating concrete environment, J. Electroanal. Chem. 736 (2015) 38–46.

[22] D.A. Koleva, J.H.W. de Wit, K. van Breugel, Z.F. Lodhi, G. Ye, Investigation of Corrosion and Cathodic Protection in Reinforced Concrete, J. Electrochem. Soc. 154 (2007) C261.

[23] D.A. Koleva, Electrochemical behavior of corroded and protected construction steel in cement extract, Mater. Corros. 62 (2011) 240–251.

[24] D.A. Koleva, N. Boshkov, K. van Breugel, J.H.W. de Wit, Steel corrosion resistance in model solutions, containing waste materials, Electrochim. Acta. 58 (2011) 628–646.

[25] A. Brenna, L. Lazzari, M. Ormellese, Stray current control by a new approach based on current monitoring on a potential probe, Corros. Eng., Sci. Technol. 52 (2017) 359–364.

[26] M. Ormellese, S. Goidanich, L. Lazzari, Effect of AC interference on cathodic protection monitoring, Corros. Eng., Sci. Technol. 46 (2011) 618–623.

[27] S. Sathiyanarayanan, P. Natarajan, K. Saravanan, S. Srinivasan, G. Venkatachari, Corrosion monitoring of steel in concrete by galvanostatic pulse technique, Cem. Concr. Compos. 28 (2006) 630–637.

[28] P. Giménez, K. Mukai, K. Asaka, K. Hata, H. Oike, T.F. Otero, Capacitive and faradic charge components in high-speed carbon nanotube actuator, Electrochim. Acta 60 (2012) 177–183.

[29] L. Zhu, L. Zhang, A.V. Virkar, Measurement of ionic and electronic conductivities of Yttria-stabilized zirconia by an embedded electrode method, J. Electrochem. Soc. 162 (2015) F298–F309.

[30] V.B. Svetovoy, R.G.P. Sanders, M.C. Elwenspoek, Transient nanobubbles in short-time electrolysis, J. Phys: Condens. Matter. 25 (2013).

[31] A. Lamibrac, G. Maranzana, O. Lottin, J. Dillet, J. Mainka, S. Didierjean, A. Thomas, C. Moyne, Experimental characterization of internal currents during the start-up of a proton exchange membrane fuel cell, J. Power. Sources 196 (2011) 9451–9458.

[32] L. Zhang, L. Zhu, A.V. Virkar, Electronic conductivity measurement of yttria-stabilized zirconia solid electrolytes by a transient technique, J. Power. Sources 302 (2016) 98–106.